



Preparation and evaluation of a macroporous molecularly imprinted hybrid silica monolithic column for recognition of proteins by high performance liquid chromatography

Zian Lin^{a,c,*}, Fan Yang^a, Xiwen He^a, Xiaomiao Zhao^a, Yukui Zhang^{a,b}

^a College of Chemistry, Nankai University, Tianjin 300071, China

^b National Chromatographic Research and Analysis Center, Dalian Institute of Chemical Physics, Chinese Academy of Sciences, Dalian 116023, China

^c Ministry of Education Key Laboratory of Analysis and Detection for Food Safety, Fuzhou University, Fuzhou, Fujian 350002, China

ARTICLE INFO

Article history:

Received 25 April 2009

Received in revised form 2 October 2009

Accepted 7 October 2009

Available online 26 October 2009

Keywords:

Molecular imprinting

Protein

Hybrid silica-based monolith

Organic polymer-based monolith

ABSTRACT

A novel type of macroporous molecularly imprinted hybrid silica monolithic column was first developed for recognition of proteins. The macroporous silica-based monolithic skeleton was synthesized in a 4.6 mm i.d. stainless steel column by a mild sol–gel process with methyltrimethoxysilane (MTMS) as a sole precursor, and then vinyl groups were introduced onto the surface of the silica skeleton by chemical modification of γ -methacryloxypropyltrimethoxysilane (γ -MAPS). Subsequently, the molecularly imprinted polymer (MIP) coating was copolymerized and anchored onto the surface of the silica monolith. Bovine serum albumin (BSA) and lysozyme (Lyz), which differ greatly in molecular size, isoelectric point, and charge, were representatively selected for imprinted templates to evaluate recognition property of the hybrid silica-based MIP monolith. Some important factors, such as template–monomer molar ratio, total monomer concentration and crosslinking density, were systematically investigated. Under the optimum conditions, the obtained hybrid silica-based MIP monolith showed higher binding affinity for template than its corresponding non-imprinted (NIP) monolith. The imprinted factor (IF) for BSA and Lyz reached 9.07 and 6.52, respectively. Moreover, the hybrid silica-based MIP monolith displayed favorable binding characteristics for template over competitive protein. Compared with the imprinted silica beads for stationary phase and in situ organic polymer-based hydrogel MIP monolith, the hybrid silica MIP monolith exhibited higher recognition, stability and lifetime.

© 2009 Elsevier B.V. All rights reserved.

1. Introduction

Molecular imprinting is a technique, which involves the formation of recognition sites in a synthetic polymer matrix that are of complementary in shape, size, and functionality with respect to the template and favor the rebinding of template molecules to other compounds with similar structures [1–3]. Over the past decades, this technique has received considerable attention due to the potential applications in the fields of chromatographic stationary phases [4–6], solid-phase extraction [7,8], artificial antibody mimics [9,10], catalysis [11,12], and biosensing [13–15]. Despite the attractive features of this technique with selectivity that has been largely reserved for small molecules, imprinting biomacromolecules like protein still represents a great challenge. A number of key inherent problems in protein imprinting have been identified now, including permanent entrapment, poor mass transfer,

denaturation, and heterogeneity in binding pocket affinity [16]. In response to such limitation, diverse strategies have been addressed for protein imprinting such as bulk polymerization (3D imprinting) [17,18], epitope approach [19,20], and surface imprinting (2D imprinting) [21–23].

Among the various molecularly imprinted polymer (MIP) structures, one of specific interests is the use of the MIP as HPLC stationary phases for separation of target protein due to their uniquely predetermined selectivity [17,18,24–26]. Normally, MIP stationary phases have been prepared by bulk polymerization that needs a large number of template proteins, and the resulting polymer blocks are required for grinding, sieving and column packing. Although the process of bulk polymerization is simple, the rest of preparation steps are tedious, time-consuming and not cost-efficient. Furthermore, permanent entrapment caused by bulk polymerization often makes it difficult for template removal and reintroduction into the imprinted cavities, which would have a negative impact on the chromatographic performance. Most seriously, large amount of binding sites of the resulting particles are destroyed by mechanical process of grinding, which may greatly diminish selectivity for protein recognition [27].

* Corresponding author at: College of Chemistry, Nankai University, Tianjin 300071, China. Tel.: +86 22 23494962; fax: +86 22 23494962.

E-mail address: zalin@nankai.edu.cn (Z. Lin).

The development of MIP monolithic column is an alternative approach that may overcome to a great extent these disadvantages of the conventional MIP packed column. MIP monoliths have rapidly evolved in recent years [28–30] since Matsui et al. [31] employed an in situ polymerization technique to prepare MIP monolithic rods in 1993. Depending on the monolithic material, the MIP monolithic matrix can be divided into organic polymer-based [32] and silica-based monolith [33]. The former has been extensively investigated because of the easy fabrication by single-step polymerization reaction, good biocompatibility and excellent pH stability. The latter can be prepared with independent control of silica skeletons and macropores via a sol–gel process, offering high permeability, high mechanical strength, high efficiency, and good solvent resistance. Besides, silica-based monoliths are not apt to swell or shrink in different organic mobile phases [34]. Up to date, however, only one publication [33] reported on the preparation of a silica-based MIP capillary monolithic column for enantioseparation of small molecules since the sol–gel process is difficult to control and often associated with the cracking and shrinking of silica skeleton during drying. To solve these difficulties, Wang et al. [35] have developed an attractive method for fabrication of a hybrid silica-based MIP capillary monolith based on room temperature ionic liquid-mediated, non-hydrolytic sol–gel process, with which chiral separation of naproxen has been achieved by capillary electrochromatography. This hybrid monolith, as well as possessing the merits of organic polymer- and silica-based monolith does not require aging and drying steps at high temperature, avoiding the cracking and shrinking of the silica skeleton.

This work focused on the development of a novel hybrid silica-based MIP monolith technology and its first application in protein recognition. To the best of our knowledge, preparation and application of the hybrid silica-based MIP monolith for protein recognition have not been reported yet. Characterization of the prepared MIP monolith was described in detail. Furthermore, the recognition property of the prepared hybrid silica-based MIP monolith was evaluated by imprinting different templates. Compared with the imprinted silica beads and in situ organic polymer-based hydrogel MIP monolith, the hybrid silica MIP monolith exhibited better chromatographic performances.

2. Experimental

2.1. Materials

Bovine serum albumin (BSA), human serum albumin (HSA), bovine hemoglobin (BHb), ovalbumin (OB) and lysozyme (Lyz) were purchased from Shanghai Lanji Co. Ltd. (Shanghai, China). Methyltrimethoxysilane (98%, MTMS) and γ -methacryloxypropyltrimethoxysilane (γ -MAPS) were obtained from Sigma (St. Louis, MO). Acrylamide (AM), N,N'-methylenebisacrylamide (BisAM), and N,N,N,N'-tetramethylethylenediamine (TEMED) were the products of Qianjin Chemistry Reagent Factory (Tianjin, China). Ammonium persulfate (APS) and sodium dodecyl sulfate (SDS) were obtained from institute of Tianjin Guangfu Chemicals (Tianjin, China). Silica beads (20–40 μ m, Tiajin Chromatography Technology Company) were activated with acid prior to use. Deionized water was prepared with a Milli-Q water purification system (Millipore, Milford, MA). Different sizes of stainless steel columns were supplied by Puxiang chromatogram equipment Co., Ltd. (Tianjin, China), which was utilized for preparation of the hybrid silica-based MIP monolith (100 mm \times 4.6 mm i.d.) and the organic polymer-based MIP monolith (150 mm \times 4.6 mm i.d.).

2.2. Instruments

All the chromatographic experiments were performed on a Shimadzu SPD-M20A HPLC system (Shimadzu, Japan), which con-

sisted of a DGU-20A₅ on-line degasser, a LC-20AD HPLC pump, as well as a diode array detector. The data were acquired and processed with an LCsolution chromatographic workstation (Shimadzu, Japan). The scanning electron micrographic (SEM) images of the monoliths were obtained by a SS-550 scanning electron microscope (Shimadzu, Japan). Fourier Transform Infrared (FT-IR) spectra (4000–400 cm^{-1}) in KBr were recorded using the AVATAR 360 FT-IR spectrophotometer (Nicolet, Waltham, USA). Circular dichroism (CD) experiments were carried out on a spectropolarimeter (JASCO, model J-810 United Kingdom). UV/vis spectra (200–850 nm) were obtained by using UV-2450 spectrophotometer (Shimadzu, Japan). Pore-size distribution measurements were conducted on an AutoPoreIV 9500 mercury intrusion porosimetry (Micromeritics, Norcross, GA, USA). Elemental analysis of monolithic materials was carried out on CHNOS Elemental analyzer (Vario MICRO, Elementar, Germany).

2.3. Preparation of hybrid silica-based MIP monolithic column

2.3.1. Preparation of macroporous silica skeleton

The silica monolithic skeleton in a stainless steel column was prepared as described by Laschober et al. [36] with some modifications. Briefly, 2.0 mL of MTMS, 0.75 mL of anhydrous methanol (MeOH) and 0.5 mL of 1.0 mol/L nitric acid were mixed in polypropylene vessel. The solution was stirred at room temperature for approximate 2 min and then poured into a stainless steel column with closed outlet at the bottom. With another end sealed by parafilm, the column was vertically placed in oven at 40 °C for overnight. After gelation the column was rinsed with MeOH and then dried at 40 °C for chemical modification in the next step.

2.3.2. Chemical modification of γ -MAPS on the surface of the silica skeleton

Prior to modification, the silica monolithic column was rinsed with 0.1 mol/L HCl solution for 5 h and then with water until the pH value of outlet solution was 7.0. After subsequent flushing with MeOH for 30 min, it was dried by passage of nitrogen gas. The solution of γ -MAPS in anhydrous MeOH (1/1, v/v) was continuously pumped into the monolithic column for 2 h with the LC pump at a constant flow rate of 0.05 mL/min and kept at 40 °C for overnight. Finally, the monolithic column was sequentially rinsed with MeOH, and dried again.

2.3.3. Polymerization of MIP coating onto the surface of the modified silica skeleton

The template (Lyz or BSA), functional monomer (AM), as well as crosslinker (BisAM) were mixed and dissolved with 20 mL deionized water. After placing for 1 h at room temperature, the solution was degassed under nitrogen for about 3 min to eliminate soluble oxygen. The crosslinking density ($C\%$) and the total monomer concentration ($T\%$) (For definition of T and C , see Ref. [26]) were listed in Table 1. After adding initiator (40 mg APS), the solution was pumped into the modified silica monolithic column with the flow rate of 0.05 mL/min for 2 h under ice bath. Sequentially, the polymerization proceeded at room temperature for overnight. The non-imprinted (NIP) silica monolith was also prepared in the absence of template by using the same preparation procedure as described above.

2.4. Preparation of organic polymer-based hydrogel MIP monolith

According to the same composition of $C\%$ and $T\%$ as described in Table 1, in situ polymerization of the organic polymer-based hydrogel MIP monolithic column was also performed. In brief, 20.6 mg Lyz (or 79.5 mg BSA), 880 mg AM (or 660 mg for BSA), and 120 mg BisAM

Table 1
Conditions for preparation of Lyz-MIP hybrid silica-based monolithic column.

Columns	Template/monomer molar ratio ^a	AM (mg)	BisAM (mg)	C %	T %	H ₂ O (mL)	(NH ₄) ₂ S ₂ O ₈ (mg)
A1	1/8000	3680	320	8	20	20.0	40.0
A2	1/8000	3600	400	10	20	20.0	40.0
A3	1/8000	3520	480	12	20	20.0	40.0
A4	1/8000	3400	600	15	20	20.0	40.0
A5	1/8000	1760	240	12	10	20.0	40.0
A6	1/8000	2640	360	12	15	20.0	40.0
A7	1/8000	4400	600	12	25	20.0	40.0
A8	1/4000	3520	480	12	20	20.0	40.0
A9	1/12000	3520	480	12	20	20.0	40.0

^a The template–monomer molar ratio for preparation of BSA-MIP hybrid silica monolith is 1/4000; other experimental conditions are same as Lyz-MIP monolith.

(or 90 mg for BSA) were dissolved in 5 mL deionized water and degassed under nitrogen for 3 min after placing for 1 h. Following addition of 10 mg of APS, 3 μ L of TEMED solution as an accelerator was added and stirred for 10 s. Then, the reaction mixture was swiftly introduced into stainless steel column. The polymerization solution in the stainless steel column was frozen at -20°C for 12 h and thawed at room temperature, and thus the porous hydrogel monolith could be obtained.

2.5. Preparation of imprinted silica beads

The dried silica beads (10 g) were dissolved with 10 mL of γ -MAPS in MeOH (1/1, v/v) and stirred at room temperature for 24 h under nitrogen protection. Then the silica beads were filtered out and washed successively with MeOH and water. The modified silica beads were dried under vacuum at 50°C for overnight.

20.6 mg Lyz (or 79.5 mg BSA), 880 mg AM (or 660 mg for BSA), 120 mg BisAM (or 90 mg for BSA) and 1.0 mg of γ -MAPS-modified silica beads were dissolved in 5 mL deionized water and was incubated for 1 h at room temperature. The polymerization was initiated by adding 10 mg of APS and 3 μ L of TEMED solution. Polymerization was continued at -20°C for 12 h and MIP silica beads were obtained. After grinding and sieving, the MIP silica beads were packed into column.

2.6. Spectral characterization

1.0 mL, 0.01 mg/mL Lyz (or 0.02 mg/mL for BSA) solution prepared with deionized water was added to the equal volume of 0.4 mg/mL AM-BisAM (or 0.2 mg/mL for BSA) solution. Then the mixtures were loaded into a 5 mm round cuvette and were analyzed by CD spectropolarimeter with continuous mode, at a scan speed of 50 nm/min. The range of wavelength scanned was from 195 nm to 250 nm. In addition, the obtained hybrid silica-based MIP monolithic column was flushed with 1% (w/v) SDS in order to remove template. The solution was passed through the MIP monolithic column by LC pump at the flow rate of 0.05 mL/min over 24 h (about 48 h for imprinted silica beads and organic polymer-based MIP monolith). This procedure was continued until no template protein was detected in the washing solution. The protein leakage was followed by monitoring the absorbance in UV/Vis spectrophotometer at 280 nm.

2.7. Separation conditions of HPLC

In order to avoid the collapse of the organic polymer-based hydrogel MIP monolith and maintain the stability of recognition sites, low flow rate of mobile phase with 0.05 mL/min was recommended. The injected volume was 20 μ L and the detec-

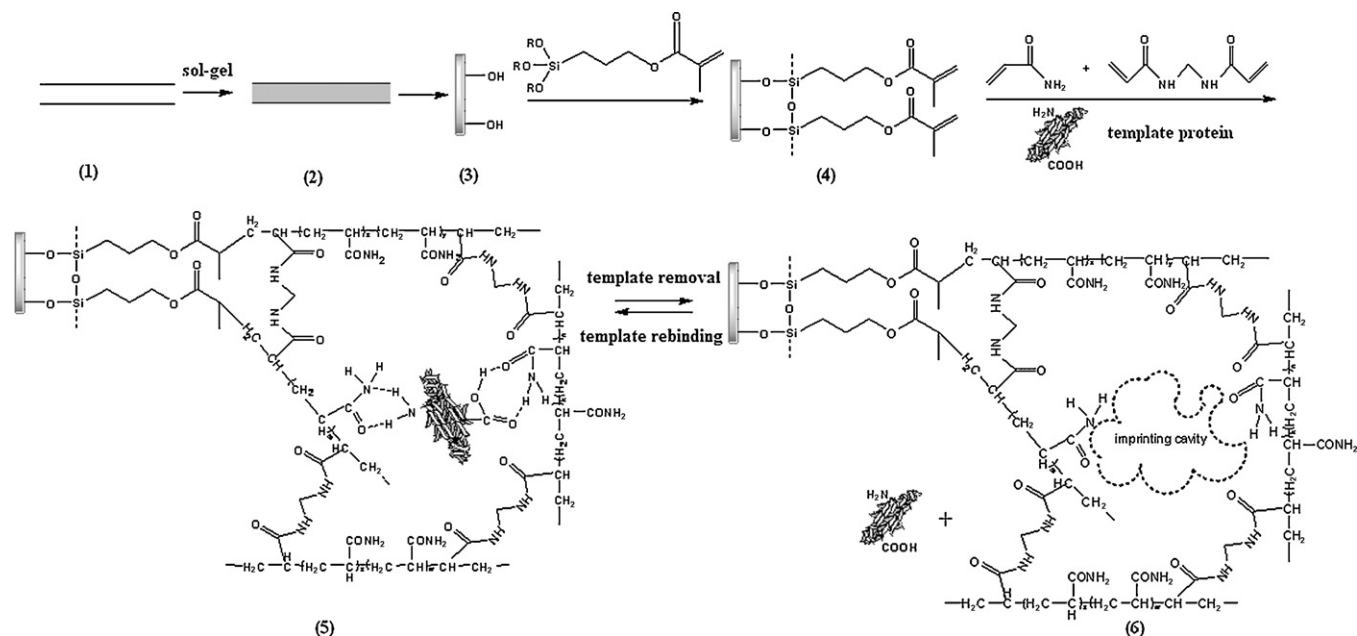


Fig. 1. Schematic representation of preparation procedures of hybrid silica-based MIP monolithic column. (1) Bare stainless steel column; (2) naked silica skeleton prepared by sol-gel process; (3) silanols on the surface of silica monolith; (4) vinylation on the surface of silica monolith; (5) formation of MIP coating on the surface of silica monolith; (6) removal of template protein.

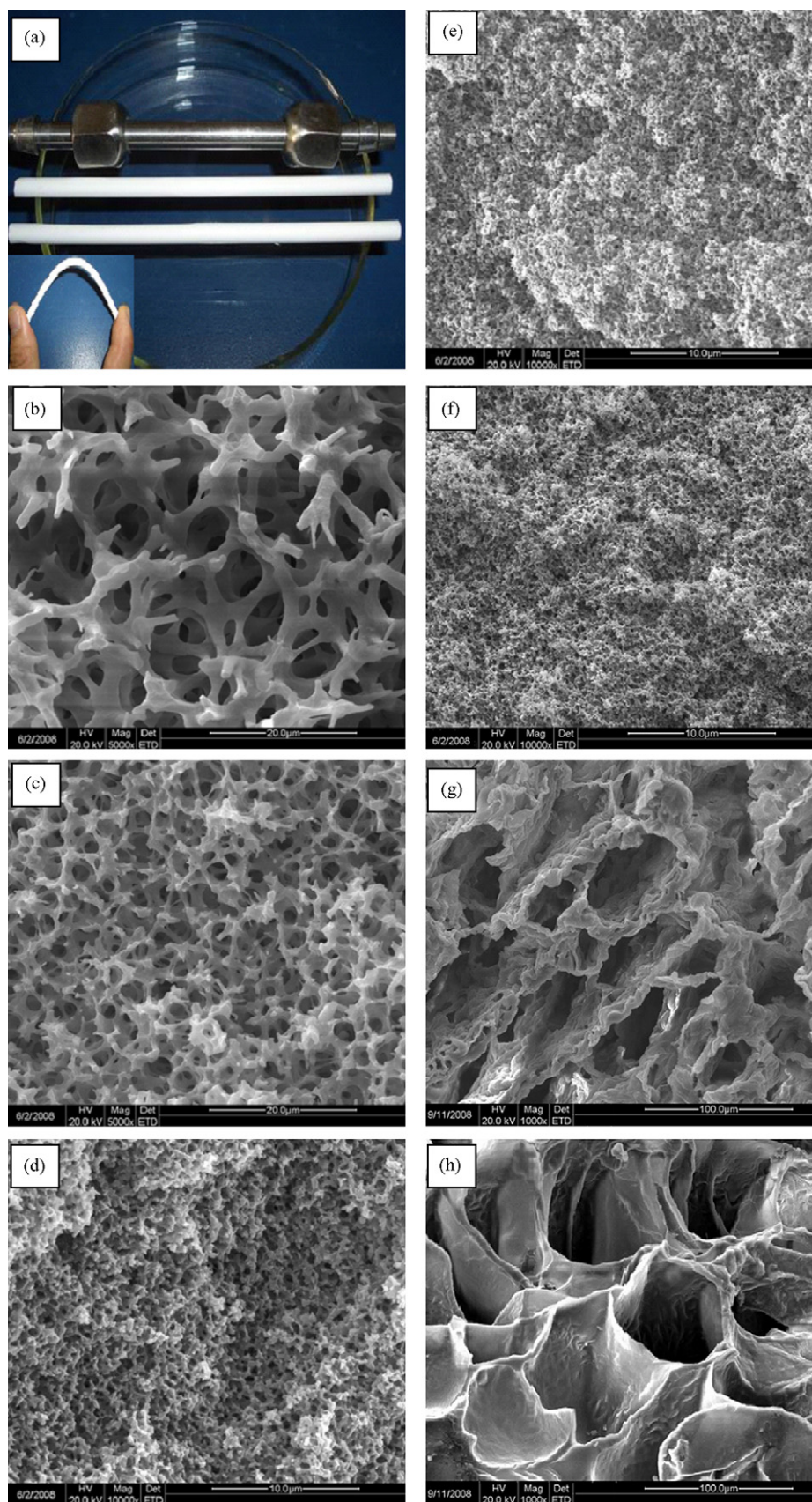


Fig. 2. (a–h) Photographs of the prepared hybrid silica-based and organic polymer-based MIP monolithic column. (a) Preparation of naked silica skeleton, (b) SEM image of naked silica skeleton, (c) after modification of γ -MAPS, (d) hybrid silica-based NIP monolith, (e) Lyz-MIP hybrid silica-based monolith, (f) BSA-MIP hybrid silica-based monolith, (g) Lyz-MIP organic polymer-based monolith, (h) BSA-MIP organic polymer-based monolith.

Table 2
The properties of hybrid silica-based MIP monolithic column synthesized at the optimized conditions^a.

Columns	Average pore diameter (nm)	Surface areas (m ² /g)	V _{pore} (mL/g)	Pressure drop (MPa) ^b
Silica skeleton	8902	28.6	1.56	0.5
γ-MAPS-modified monolith	1083	38.2	1.34	0.8
Lyz-NIP	237	53.9	1.11	1.2
Lyz-MIP	145	64.6	1.19	1.2
BSA-NIP	210	51.7	1.03	1.2
BSA-MIP	182	58.2	1.15	1.2

^a Experimental conditions: C = 12%, T = 20% for Lyz-template monolith; C = 12%, T = 15% for BSA-template monolith.

^b The pressure drop was measured at a constant flow rate of 0.5 mL/min from an HPLC pump using water.

tion wavelength was set at 280 nm. Mobile phases were prepared by mixing different volumes of disodium hydrogen phosphate and sodium dihydrogen phosphate, which needed to be filtered through a 0.45 μm membrane (Nihon Millipore Ltd.) and degassed by vacuum prior to use. Sample solutions were dissolved in the mobile phase with the content of 1.0 mg/mL and stored at +4 °C. The retention factor, *k*, were calculated using the equation $k = (t_R - t_0)/t_0$, where *t_R* is the retention time of the protein and *t₀* is the elution time of void marker (acetone). The imprinted factor (IF) ($IF = k_{MIP}/k_{NIP}$) was defined as the ratio of the retention factor of template protein in MIP monolith and NIP monolith, which was adopted for evaluation of the imprinting ability. The separation factor (*α*) was calculated according to the equation $\alpha = k_{tem}/k_{con}$, where *k_{tem}* and *k_{con}* are the retention factor of template and competitive protein in MIP or NIP monolith, respectively. The *k* and *α* were determined by the injection of a single component. The resolution (*R_s*) was calculated from the equation $R_s = 2(t_2 - t_1)/(W_1 + W_2)$, where *t₁* and *t₂* are the retention time of the competitive protein and template protein. *W₁* and *W₂* are the baseline peak widths of competitive protein and template protein, respectively.

3. Results and discussion

3.1. Preparation and SEM characterization of hybrid silica-based MIP monolithic column

The general scheme for preparation of the hybrid silica-based MIP monolithic column was illustrated in Fig. 1, which included four steps: (a) preparation of silica skeleton, (b) chemical modification with γ-MAPS, (c) polymerization of functional monomer and crosslinker at the surface of silica skeleton, (d) removal of template to form MIP monolith.

In our experiments, a mild sol-gel approach was adopted for preparing silica skeleton, by which the surpermacroporous structure of the silica skeleton could be obtained. MTMS was utilized as a sole organic-inorganic hybrid precursor to eliminate the shrinkage of silica skeleton that often encountered with tetramethoxysilane (TMOS) as precursor during aging and drying. MeOH was added to the reaction solution, not only to dissolve the rather apolar precursor, but also to act as porogen for the formation of an appropriate surpermacroporous structure. Under the optimum conditions (V_{MTMS}:V_{MeOH}:V_{HNO₃} = 2.0 mL:0.75 mL:0.5 mL), the obtained silica monolithic rod has not obvious shrinkage in dimension as shown in Fig. 2(a). Furthermore, the prepared silica monolithic rod with MTMS was more flexible than that of TMOS, which enabled the silica rod to endure the stress generated by the shrinkage and could suppress the formation of the voids.

Fig. 2(b) illustrates the SEM photograph of the naked silica monolithic skeleton with a diameter of 4.6 mm. It can be observed that the monolithic column has the morphology of a continuous skeleton and surpermacropores of ~10 μm. The surpermacroporous silica skeleton not only results in low backpressure and high

permeability, but also provides enough spaces for further chemical modifications.

For acquiring a stable MIP coating onto silica monolith, vinylation of the surface of silica monolithic skeleton was introduced by chemical modifications with γ-MAPS. Although the amount of surpermacropores markedly decreased after modifications (see Fig. 2(c)), the large through-pores in the size range of 1–2 μm still dominantly existed that may provide the fast mass transfer from mobile phase to stationary phase, so high column efficiency could be expected.

Fig. 2(d–f) shows the SEM photographs of NIP and MIP silica-based monolithic column. Due to the organic MIP as soft gels grafted onto the surface of the modified silica skeleton, the images observed from the cross section of the silica skeleton become obscure. The denser and smaller pores were formed after copolymerization of AM, BisAM and γ-MAPS by the initiator of APS, which could offer larger surface area and recognition sites that were desirable for the selective rebinding of the template. Compared to the conventional capillary monolith (pore diameter: ~nanometer), the pores of hybrid MIP monolith was submicrometer-sized structure and higher permeability could be expected. The data of pressure drop of the prepared hybrid MIP monolith were listed in Table 2. Additionally, the morphology of this composite monolith is different from the particulate structure of an organic polymer-based MIP monolith, whose SEM photograph is displayed in Fig. 2(g–h). After drying at vacuum, the pore structures of the NIP and MIP silica-based monoliths were measured by mercury intrusion porosimetry and these results (see Table 2) validated that the slight discrimination existed in NIP and MIP monolith.

3.2. Elemental analysis

To ascertain each modification, elemental analysis was employed and the results were shown in Table 3. After chemical modification of γ-MAPS, the carbon composition increased from 14.13 to 15.73, suggesting the vinyl groups were successfully introduced onto the surface of the silica skeleton. After polymerization, the nitrogen compositions of Lyz-MIP and BSA-MIP monoliths were 2.56 and 2.13, respectively. Different C % and T % contributed to the different nitrogen compositions. In addition, the corresponding nitrogen compositions of NIP monolith for Lyz and BSA were 2.39 and 1.98, slightly lower than its MIP monolith. Possible reason was that the template protein was not completely extracted from the MIP monolith.

Table 3
Elemental analysis of hybrid silica-based Lyz-MIP and BSA-MIP monoliths.

Each step	C (%)	H (%)	N (%)
Silica skeleton	14.13	4.40	0
γ-MAPS-modified monolith	15.73	4.57	0
Lyz-MIP	17.89	4.79	2.56
Lyz-NIP	17.75	4.81	2.39
BSA-MIP	16.80	4.33	2.13
BSA-NIP	16.63	4.15	1.98

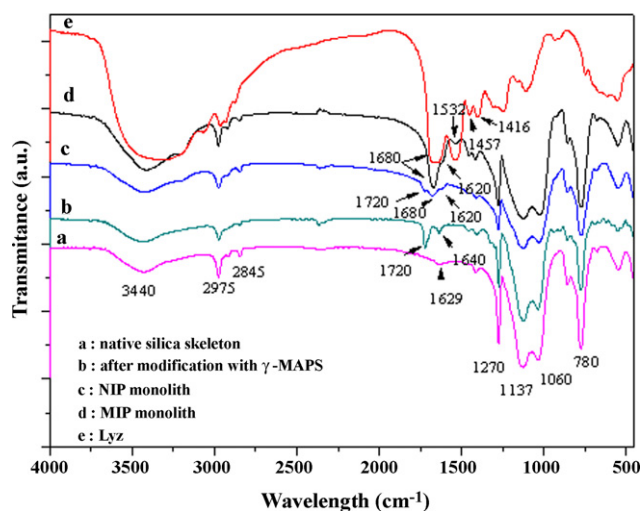


Fig. 3. FT-IR spectra of the (a) naked silica skeleton, (b) after modification of γ -MAPS, (c) hybrid silica-based NIP monolith, (d) hybrid silica-based MIP monolith, (e) Lyz.

3.3. Spectral characterization of hybrid silica-based MIP monolithic column

To further determine the characteristics of the hybrid silica-based MIP monolithic column, FT-IR spectra of the naked silica skeleton, γ -MAPS-modified silica skeleton, silica-based NIP and MIP monolith after copolymerization of AM and BisAM, together with the spectrum of Lyz, were compared in Fig. 3. The strong peaks near 1137 and 1060 cm^{-1} were assigned as the Si–O–Si asymmetric stretches and the features around 3440 and 1629 cm^{-1} were attributed to –OH vibrations in the bulk gel. The bands at 1720 and 1640 cm^{-1} were C=O stretch and C=C stretch (spectra b), suggesting that the γ -MAPS has been successfully modified onto the surface of the naked silica skeleton. The NIP and MIP silica monoliths show similar locations and appearances of the major bands (spectra c and d). Characteristic features of the NIP and MIP monoliths when compared with the modified silica skeleton were a –CO–NH₂ bond around 1680 cm^{-1} and N–H bond around 1620 cm^{-1} . Moreover, the band at 1640 cm^{-1} for C=C stretch disappeared. These results confirm that AM and BisAM had been successfully grafted onto the surface of silica skeleton by polymerization of carbon–carbon double bonds between AM, BisAM, and γ -MAPS. Besides, many same characteristic peaks were observed by comparing spectra d and spectra e (e.g. 1680, 1532, 1457, and 1416 cm^{-1}), which indicates the template is interacting with AM by non-covalent binding. From these FT-IR spectra, however, it is difficult to determine whether the template was removed after extraction because of the low concentration of the template in bulk polymer.

To ascertain the removal of template protein from MIP silica monolith, SDS was selected as eluent in this work, because the SDS has proven to be an excellent denaturation solvent for protein imprinting in the aqueous phase [37]. Fig. 4 demonstrates that the UV spectra of Lyz-imprinted and non-imprinted solution after elution. With the increase of elution time, the absorbance of Lyz evidently decreased at the detection wavelength of 280 nm. No template could be detected until the elution time reached over 20 h. The result confirms the efficient removal of the template from the MIP monolithic column.

In the noncovalent approach of molecular imprinting, the formation of binding sites depends on the interaction of the template with the complementary functional moieties of the monomers at certain spatial positions. This indicates the importance of the

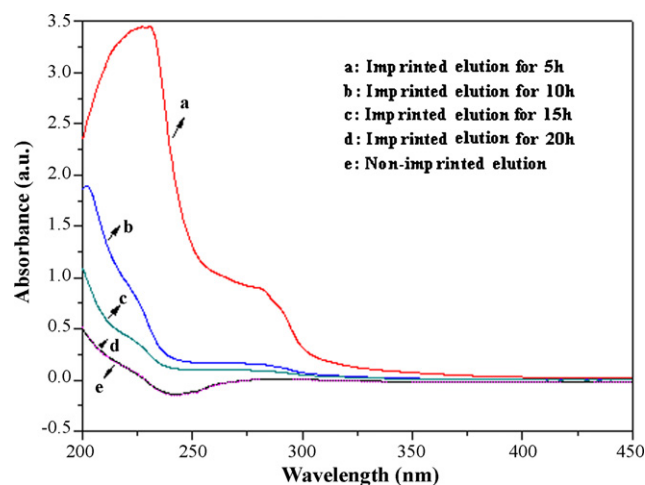


Fig. 4. UV spectra of the Lyz after elution (a) elution for 5 h, (b) elution for 10 h, (c) elution for 15 h, (d) elution for 20 h, (e) NIP elution.

structural characteristics of the template. An investigation on the possible denaturation of template protein in imprinting mixture needs to be performed by using CD. As shown in Fig. 5(a and b), the CD spectrum for Lyz or BSA in imprinting mixture (curve (3))

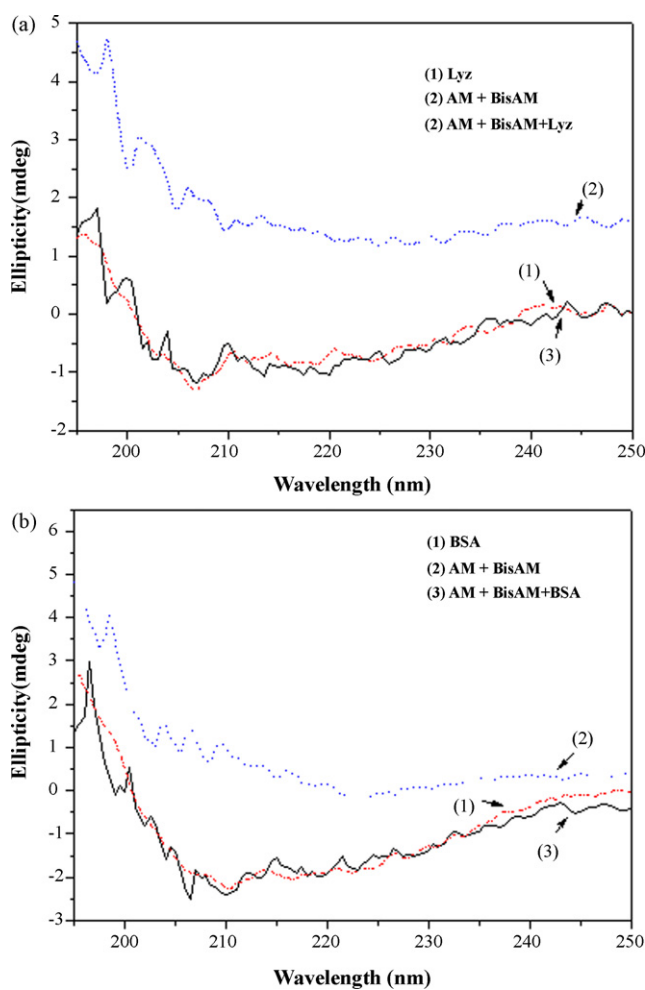


Fig. 5. (a and b) CD spectra of Lyz (a) and BSA (b) at the AM-BisAM solutions. (a) (1) 0.005 mg/mL Lyz; (2) 0.2 mg/mL AM-BisAM solution; (3) 0.005 mg/mL Lyz + 0.2 mg/mL AM-BisAM solution. (b) (1) 0.01 mg/mL BSA; (2) 0.1 mg/mL AM-BisAM solution; (3) 0.005 mg/mL BSA + 0.1 mg/mL AM-BisAM solution.

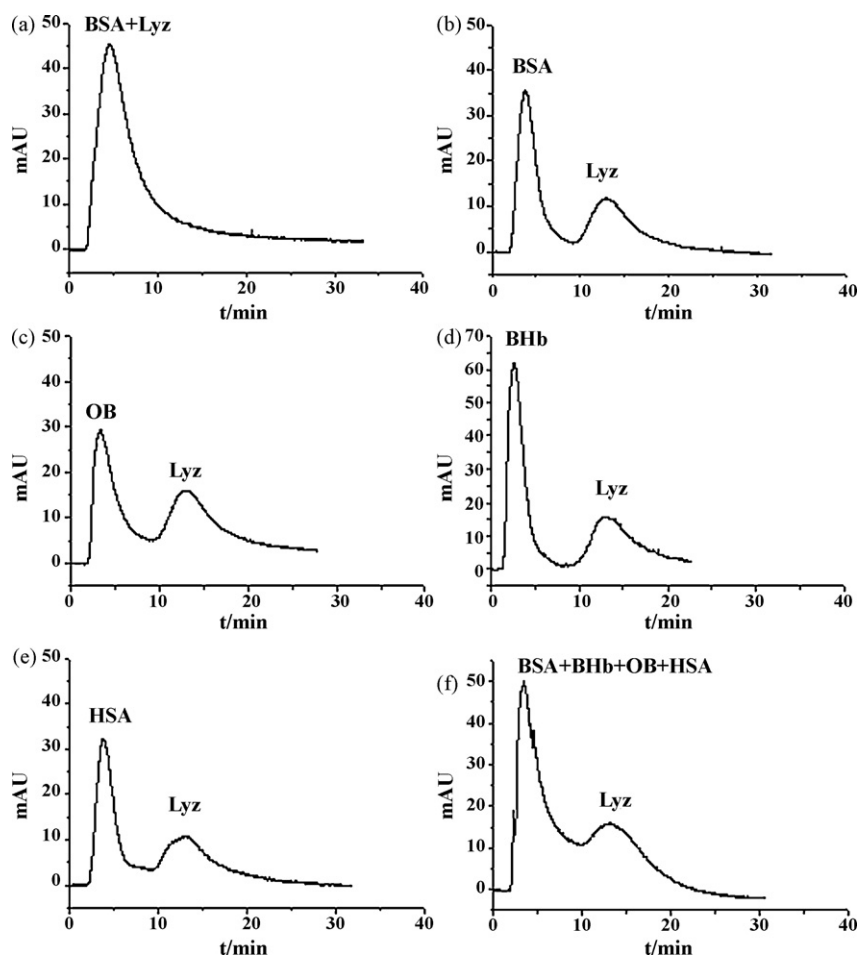


Fig. 6. (a–f) Separation of competitive proteins and Lyz on hybrid silica-based NIP (a) and Lyz-MIP monolith (b–f). Experimental conditions: NIP and Lyz-MIP monolith, $C = 12\%$, $T = 20\%$; mobile phase, 25 mmol/L phosphate buffer (pH 7.0); flow rate, 0.05 mL/min; column pressure: 0.3 MPa; stainless steel column, 100 mm \times 4.6 mm i.d. detection wavelength, 280 nm; (a–e) $C_{\text{BSA}} = C_{\text{BHb}} = C_{\text{OB}} = C_{\text{HSA}} = C_{\text{Lyz}} = 1.0$ mg/mL; (f) $C_{\text{BSA}} = C_{\text{BHb}} = C_{\text{OB}} = C_{\text{HSA}} = 0.25$ mg/mL, $C_{\text{Lyz}} = 1.0$ mg/mL.

remained almost identical to that of a native one (curve (1)), and the α helix could be observed at the wavelength of 208 nm, which implied that the AM-BisAM solution did not pose any significant effect on the protein configuration.

3.4. Selective separation of protein on the hybrid silica-based MIP monolithic column

To evaluate the selectivity of the prepared hybrid silica-based MIP monoliths for template protein, Lyz and BSA were selected as imprinted templates, respectively. Fig. 6(a–f) shows the chromatographic separation of template (Lyz) and competitive proteins (including BSA, BHb, OB, and HAS) on the NIP and Lyz-MIP monolithic column. With the composition of the 12% C and 20% T (see Table 1, column A3), the retention factor (k) for Lyz on the Lyz-MIP monolith was 4.04, much higher than that obtained on the NIP monolith, where the k was 0.62. The imprinted factor of Lyz reached 6.52. On the other hand, the Lyz-MIP monolith exhibited a high selectivity degree versus Lyz with respect to the competitive proteins, and near baseline separation was achieved. Additionally, good recognition for template from complex mixture was also shown in Fig. 6(f). These results could be explained by the fact that the imprinting process in Lyz-MIP monolith could form recognition sites that were complementary in shape, size, and functionality with respect to the template and preferentially recognized Lyz. So the strong retention for Lyz in Lyz-MIP monolithic column could be obtained. Contrarily, the non-specific adsorption had dominant

effect in the NIP monolith due to lack of imprinting process. It is difficult for the NIP monolith to form recognition cavities and the interaction between the binding sites and Lyz is weak. Therefore, the NIP monolith did not display any recognition ability for template and the k is nearly close to the void fraction.

Similar results were obtained while using BSA as imprinted template, where the composition of BSA-MIP monolith was 12% C and 15% T. As seen from Fig. 7(a–f), the analytes were eluted in the order of competitive proteins (Lyz, BHb, OB, and HSA) then template (BSA) on the BSA-MIP monolith. Although BSA and HSA could not be separated well, the k is different (see Fig. 7(e)). Highly similar steric conformation could respond for the result. The data of Lyz and BSA of t_R , k , R_s , IF, and α were summarized in Table 4. These results

Table 4
Chromatographic separation data of Lyz-MIP and BSA-MIP silica-based monoliths.

Columns	t_R (min) (t_0)	k	IF	α	R_s
Lyz (Lyz-MIP) ^a	13.0 (2.7)	4.04	–	–	–
Lyz (Lyz-NIP)	4.22	0.62	6.52	–	–
BSA (Lyz-MIP)	3.75	0.45	–	8.98	1.24
BSA (Lyz-NIP)	3.73	0.44	–	1.40	–
BSA (BSA-MIP) ^b	18.8 (5.3)	2.36	–	–	–
BSA (BSA-NIP)	6.70	0.26	9.07	–	–
Lyz (BSA-MIP)	7.80	0.39	–	6.05	1.01
Lyz (BSA-NIP)	6.75	0.27	–	0.96	–

Experimental conditions are same as in Figs. 6 and 7.

^a Presents Lyz in Lyz-MIP silica monolith ($C = 12\%$; $T = 20\%$).

^b Presents BSA in BSA-MIP silica monolith ($C = 12\%$; $T = 15\%$).

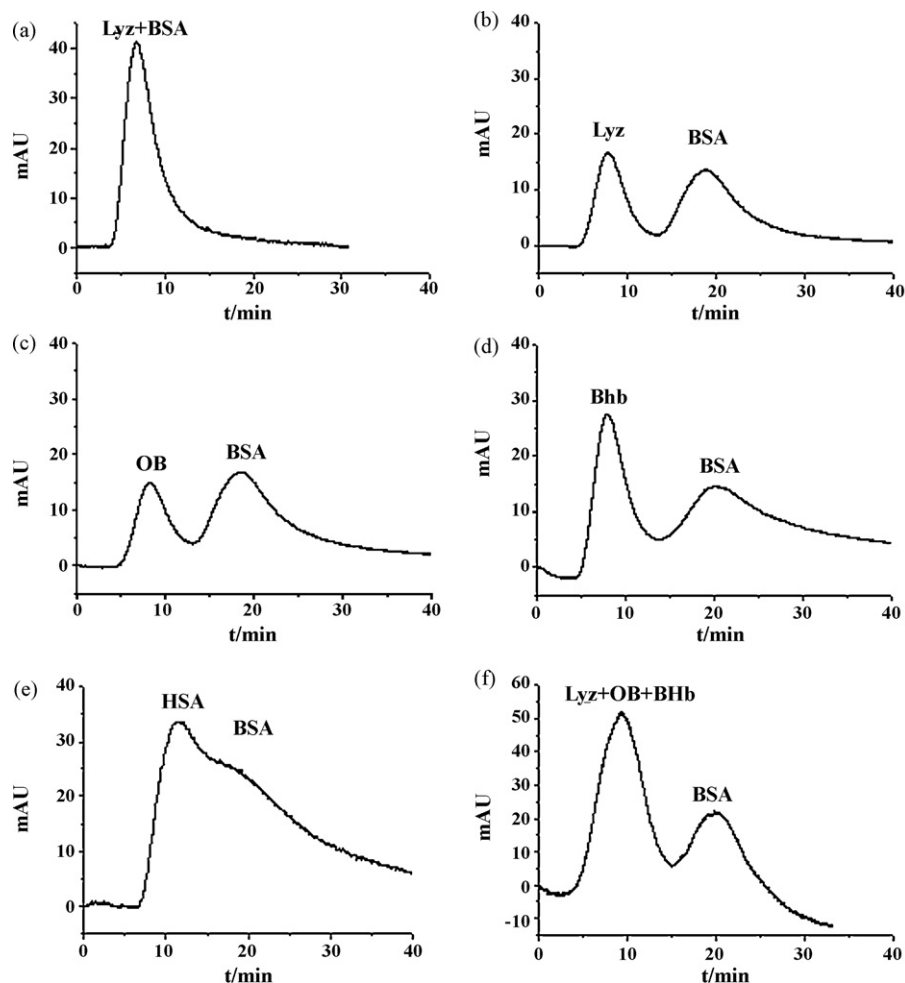


Fig. 7. (a–f) Separation of competitive proteins and BSA on hybrid silica-based NIP (a) and BSA-MIP monolith (b–f). Experimental conditions: NIP and BSA-MIP monolith, $C = 12\%$, $T = 15\%$; mobile phase, 10 mmol/L phosphate buffer (pH 7.0). Other: flow rate, 0.05 mL/min; column pressure: 0.3 MPa; stainless steel column, 100 mm \times 4.6 mm i.d. detection wavelength, 280 nm; (a–e) $C_{BSA} = C_{Bhb} = C_{OB} = C_{HSA} = C_{Lyz} = 1.0$ mg/mL; (f) $C_{Lyz} = C_{Bhb} = C_{OB} = 0.3$ mg/mL, $C_{BSA} = 1.0$ mg/mL.

indicate that the hybrid silica-based MIP monoliths have excellent recognition ability for template protein whether Lyz or BSA.

3.4.1. Effect of template–monomer molar ratio

The influence of the template–monomer molar ratio on the selectivity was investigated. Taking Lyz-MIP monolith as an example, the results (data not shown) showed that the lower or higher ratios (see Table 1, columns A8 and A9) presented low selectivity for template and corresponding chromatographic peak overlapped with competitive proteins. Major reason for this phenomenon was that the lower template–monomer ratio offered inadequate recognition cavities to bind template, but the higher ratio of template to monomer increased the non-specific binding due to the abundant exposure of peptide bonds of protein that can form hydrogen bonds with the monomer of AM. In this work, a ratio of 1:8000 was the most appropriate for the template protein.

3.4.2. Effect of crosslinking density

Traditionally, the amount of crosslinker should be high enough (>70%) in order to reduce the swelling and maintaining the stability of recognition sites [38]. This procedure is effective only for small template molecules. For protein, the degree of crosslinking has to be optimized because small pore sizes of highly crosslinked polymers will limit the access of high molecular weight proteins towards the imprinted sites. Fig. 8 illustrates the IF, α , and R_s values under the different C with Lyz-MIP monolithic column. It is seen

that the IF, α , and R_s were low when the C was 8% because the polyacrylamide gels that anchored onto the surface of the silica skeleton were too soft to form effective recognition sites. With the increase of C , the IF, α , and R_s values increased and reached its maximum at 12% C . Although high C was helpful in maintaining the shape of the

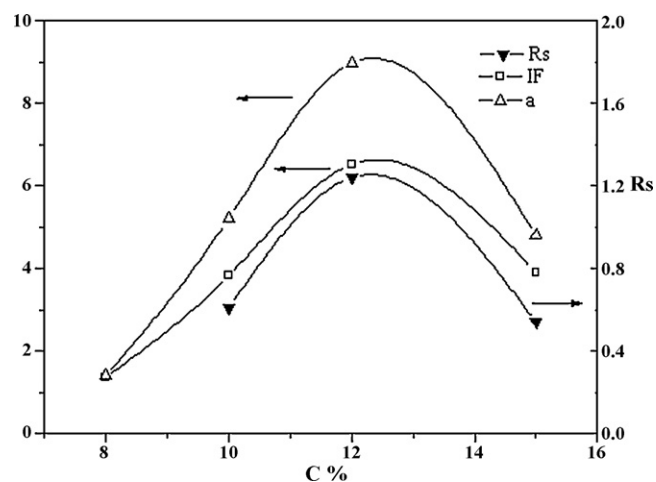


Fig. 8. Effect of different crosslinking density on the recognition of Lyz in Lyz-MIP monolith. $T = 20\%$, other HPLC conditions are same as in Fig. 6.

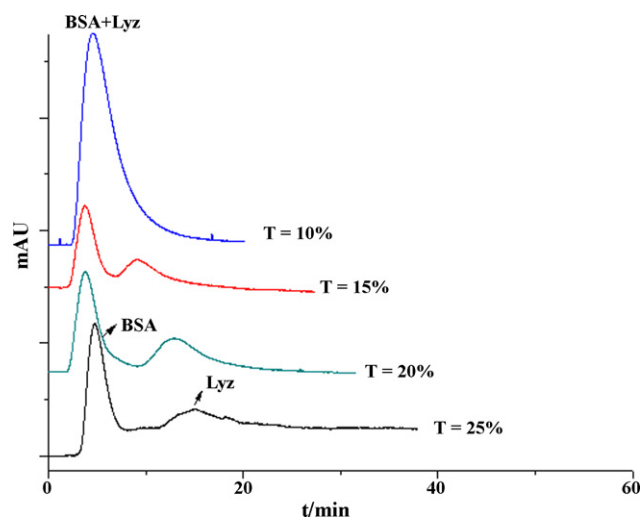


Fig. 9. Effect of total monomer concentration on the recognition of Lyz in Lyz-MIP monolith. $C = 12\%$, other HPLC conditions are same as in Fig. 6.

imprinted cavity, over-crosslinking in the polyacrylamide gels also decreased the pore radii and led to the inaccessibility of binding sites. This was the reason why the IF, α , and R_s decreased when C was higher than 12%.

3.4.3. Effect of total monomer concentration

Total monomer concentration is another important factor in imprinting protein. Keeping C constant at 12%, separation of BSA and Lyz was performed on Lyz-MIP monolith by varying T from 10% to 25%. As shown in Fig. 9, the resolution of BSA and Lyz was improved by increasing the T values. However, the extent of zone broadening and peak asymmetry of Lyz became worse with the addition of T . It can be suggested that the higher T , the stronger interaction between Lyz and AM, which favors increased recognition for Lyz, but at the expense of its column efficiency. Considering chromatographic properties (e.g. peak symmetry, resolution), 20% T was chosen for the best monomer concentration.

3.5. Selective separation of protein on the organic polymer-based hydrogel MIP monolithic column and imprinted silica beads

Fig. 10(a) illustrates the separation of the mixtures of BSA and Lyz on the Lyz-MIP and BSA-MIP organic polymer-based hydrogel monoliths under the same chromatographic conditions as in Figs. 6 and 7. By comparison, it can be seen that the resolution obtained with the hybrid silica MIP monolith was higher than that with the organic polymer-based MIP monolith. Additionally, as listed in Table 5, the IF, and α , for Lyz and BSA in the organic polymer-based MIP monolith were lower than that obtained in the

Table 5
Chromatographic separation data of Lyz-MIP and BSA-MIP organic polymer-based hydrogel monoliths.

Columns	t_R (min) (t_0)	k	IF	α	R_s
Lyz (Lyz-MIP) ^a	23.4 (10.3)	1.31	–	–	–
Lyz (Lyz-NIP)	12.3	0.26	5.04	–	–
BSA (Lyz-MIP)	13.5	0.29	–	4.52	0.48
BSA (Lyz-NIP)	11.6	0.20	–	1.30	–
BSA (BSA-MIP) ^b	26.3 (12.3)	1.11	–	–	–
BSA (BSA-NIP)	13.9	0.18	6.11	–	–
Lyz (BSA-MIP)	15.5	0.29	–	3.83	0.40
Lyz (BSA-NIP)	14.9	0.27	–	0.67	–

Experimental conditions are same as in Fig. 10(a).

^a Presents Lyz in Lyz-MIP organic polymer-based monolith ($C = 12\%$; $T = 20\%$).

^b Presents BSA in BSA-MIP organic polymer-based monolith ($C = 12\%$; $T = 15\%$).

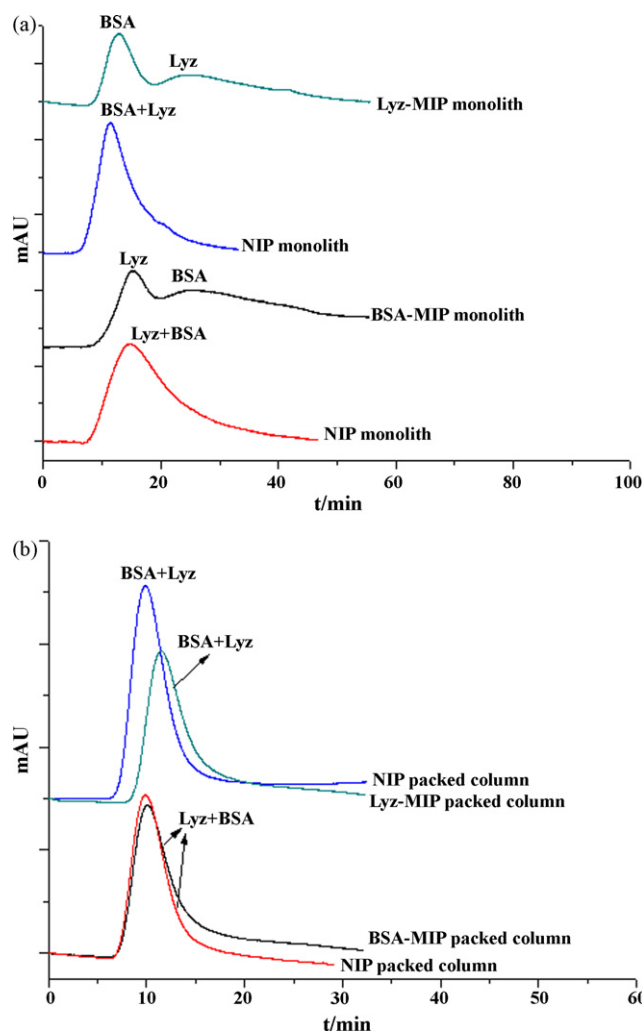


Fig. 10. (a and b) Separation of BSA and Lyz on organic polymer-based Lyz-MIP and BSA-MIP monolith (a), and on imprinted silica-bead packed column (b). Experimental conditions: (a) Lyz-MIP monolith, $C = 12\%$, $T = 20\%$; BSA-MIP monolith, $C = 12\%$, $T = 15\%$; flow rate, 0.05 mL/min; column pressure: 0.2 MPa; stainless steel column, 150 mm \times 4.6 mm i.d. (b) column pressure: 1.0 MPa; stainless steel column, 100 mm \times 4.6 mm i.d. other conditions are same as in Figs. 6 and 7.

hybrid silica MIP monolith. Possible explanation for these results was that the recognition sites of the organic polymer-based MIP monolith were created by 3D imprinting which often caused the serious entrapment of template protein and made it difficult in template reaching or leaving the formed imprinted sites. Slow association/dissociation kinetics of template with the MIP stationary phase would result in low column efficiency. Unlike the organic polymer-based hydrogel MIP monolith, the recognition sites in silica-based MIP monolith formed by 2D imprinting were situated at the surface of silica skeleton that allowed template free removal and access into the imprinted cavities. Therefore, poor mass transport and permanent entrapment was avoided, and thus high separation efficiency could be expected to obtain. In addition, the imprinted silica beads were packed into column for stationary phase and separation of both proteins are displayed in Fig. 10(b). It can be found that the Lyz-MIP and BSA-MIP packed column did not show higher binding affinity toward template than the corresponding NIP packed column, and the chromatographic peaks of Lyz and BSA overlapped absolutely. One possible reason was that the recognition sites at the surface of silica beads were destroyed after grinding, sieving and column packing.

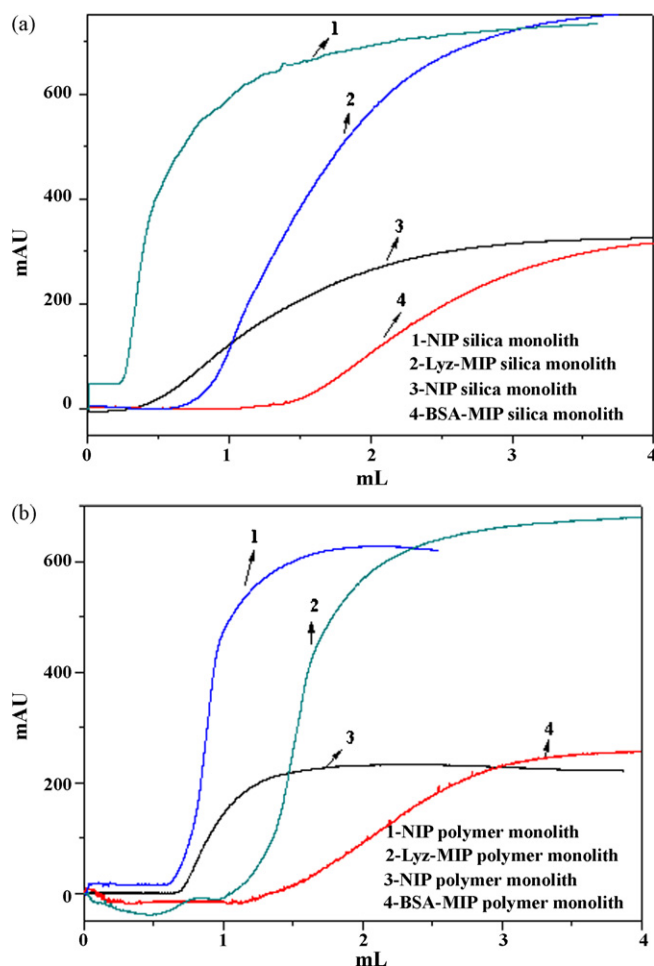


Fig. 11. (a and b) Breakthrough curve of Lyz and BSA on hybrid silica-based monolith (a), and breakthrough curve of Lyz and BSA on organic polymer-based monolith (b). Experimental conditions: Lyz-MIP monolith, $C = 12\%$, $T = 20\%$; mobile phase, 1.0 mg/mL Lyz with 25 mM phosphate buffer ($\text{pH} 7.0$); BSA-MIP monolith, $C = 12\%$, $T = 15\%$; mobile phase, 1.0 mg/mL BSA with 10 mM phosphate buffer ($\text{pH} 7.0$); other conditions are same as in Figs. 6 and 10.

3.6. Dynamic binding capacity

To determine and compare the dynamic binding capacity of NIP and MIP silica-based and organic polymer-based monoliths for template proteins, frontal analysis of the column was carried out with 1.0 mg/mL Lyz and BSA dissolved in PBS buffer ($\text{pH} 7.0$), respectively. The binding capacity (Q) was calculated by the equation [39]:

$$Q = \frac{(V_B - V_0) \times C}{m} \quad (1)$$

where V_B (mL) is the 10% background volume, V_0 is the void volumes of HPLC system, C is the protein concentration (mg/mL) and m is the weight of monolithic rod (g).

The superimposing breakthrough curves developed at the hybrid silica- and organic polymer-based monolith were shown in Fig. 11(a and b), for each template, the plot of MIP monolith was obviously departed from the NIP monolith. The dynamic binding capacities of Lyz and BSA at the organic polymer-based NIP monolith were 1.71 and 1.87 mg/g , and corresponding binding capacities at MIP monolith were 7.14 and 9.14 mg/g , respectively. On the other hand, the dynamic binding capacities of MIP hybrid silica monolith for Lyz and BSA were 6.13 and 8.92 mg/g , respectively. But the adsorptions at the NIP hybrid silica monolith were lower than those obtained at organic polymer NIP monolith due to the thin imprinted

polymer coating. The dynamic binding capacity was 1.21 mg/g for Lyz and 1.31 mg/g for BSA, indicating that the nonspecific adsorption was lower. Furthermore, the existence of specific recognition sites can respond for the difference of binding capacity between MIP and NIP monolith.

3.7. Reproducibility, stability and lifetime of hybrid silica-based MIP monolithic column

The run-to-run single column and column-to-column reproducibility were determined by measuring the k' of templates in protein-MIP monoliths. The relative standard deviations (RSDs) of run-to-run and column-to-column analysis were 5.2% ($n = 5$) and 8.6% ($n = 3$) for Lyz-MIP monolith, 4.7% and 7.8% for BSA-MIP monolith, respectively. These results suggested that the preparatory reproducibility of the hybrid silica-based MIP monolith was acceptable for the routine analysis. Since the silica-based monolithic column had a rigid skeleton, its stability and mechanical strength were high. Instead, the AM-co-BisAM polymer-based MIP monolith was a typical soft hydrogel that could not endure high pressure over 1.0 MPa . In addition, it needed to mention that no obvious decline of column efficiency was observed after hundreds of operations (~ 15 days), which was longer than the use of organic polymer-based monolith (~ 3 days). It indicated that the hybrid silica-based MIP monolith had a good lifetime.

4. Conclusions

A novel hybrid silica-based MIP monolithic column by a mild sol-gel process has been successfully developed for selective separation of proteins. The monolith integrates the merits of high selectivity of molecular imprinting and high efficiency of silica-based monolithic column. In comparison with the organic polymer-based MIP monoliths, the hybrid silica-based MIP monoliths exhibit better chromatographic performances such as recognition ability, column efficiency and so on. The purposed protein-template MIP hybrid silica monolith is expected to be a good material in selective enrichment or depletion of target protein.

Acknowledgements

We are grateful to the National Basic Research Program of China (No. 2007CB914100), China Postdoctoral Science Foundation (20070420688) and Science Start Fund of Fuzhou University (0460022233) for financial supports.

References

- [1] G. Vlatakis, L.I. Andersson, R. Müller, K. Mosbach, *Nature* 361 (1993) 645.
- [2] G. Wulff, J. Haarer, *Makromol. Chem.* 192 (1991) 1329.
- [3] C. Alexander, H.S. Andersson, L.I. Andersson, R.J. Ansell, N. Kirsch, I.A. Nicholls, J. O'Mahony, M.J. Whitcombe, *J. Mol. Recognit.* 19 (2006) 106.
- [4] R.G. Da Costa Silva, F. Augusto, *J. Chromatogr. A* 1114 (2006) 216.
- [5] M. Kempe, K. Mosbach, *J. Chromatogr. A* 694 (1995) 3.
- [6] L. Qin, X.W. He, W. Zhang, W.Y. Li, Y.K. Zhang, *J. Chromatogr. A* 1216 (2009) 807.
- [7] M.M. Ariffin, E.I. Miller, P.A.G. Cormack, R.A. Anderson, *Anal. Chem.* 79 (2007) 256.
- [8] E. Turiel, J.L. Tadeo, A. Martín-Esteban, *Anal. Chem.* 79 (2007) 3099.
- [9] S.H. Cheong, S. McNiven, A. Rachkov, R. Levi, K. Yano, I. Karube, *Macromolecules* 30 (1997) 1317.
- [10] L.I. Andersson, R. Müller, G. Vlatakis, K. Mosbach, *Proc. Natl. Acad. Sci. U.S.A.* 92 (1995) 4788.
- [11] J.Q. Liu, G. Wulff, *J. Am. Chem. Soc.* 126 (2004) 7452.
- [12] K.J. Shea, *Trends Polym. Sci.* 2 (1994) 166.
- [13] C. Malitesta, I. Losito, P.G. Zamboni, *Anal. Chem.* 71 (1999) 1366.
- [14] L. Ye, K. Mosbach, *J. Am. Chem. Soc.* 123 (2001) 2901.
- [15] K. Tappura, I. Vikholm-Lundin, W.M. Albers, *Biosens. Bioelectron.* 22 (2007) 912.
- [16] N.W. Turner, C.W. Jeans, K.R. Brain, C.J. Allender, V. Hlady, D.W. Britt, *Biotechnol. Prog.* 22 (2006) 1474.

- [17] S. Hjerten, J.L. Liao, K. Nakazato, Y. Wang, G. Zamaratskaia, H.X. Zhang, *Chromatographia* 44 (1997) 227.
- [18] D. Tong, C. Hetenyi, Z. Bikddi, J.P. Gao, S. Hjerten, *Chromatographia* 54 (2001) 7.
- [19] H. Nishino, C.S. Huang, K.J. Shea, *Angew. Chem. Int. Ed.* 45 (2006) 2392.
- [20] D.F. Tai, C.Y. Lin, T.Z. Wu, L.K. Chen, *Anal. Chem.* 77 (2005) 5140.
- [21] H.H. Yang, S.Q. Zhang, F. Tan, Z.X. Zhuang, X.R. Wang, *J. Am. Chem. Soc.* 127 (2005) 1378.
- [22] C.J. Tan, S. Wangrangsamakul, R. Bai, Y.W. Tong, *Chem. Mater.* 20 (2008) 118.
- [23] A. Bossi, S.A. Piletsky, E.V. Piletska, P.G. Righetti, A.P.F. Turner, *Anal. Chem.* 73 (2001) 5281.
- [24] T.Y. Guo, Y.Q. Xia, J. Wang, M.D. Song, B.H. Zhang, *Biomaterials* 26 (2005) 5737.
- [25] N. Bereli, M. Andaç, G. Baydemir, R. Say, T.Y. Galaev, A. Denizli, *J. Chromatogr. A* 1190 (2008) 18.
- [26] J.L. Liao, Y. Wang, S. Hjerten, *Chromatographia* 42 (1992) 259.
- [27] M. Glad, O. Norrlöw, B. Sellergren, N. Siegbahn, K. Mosbach, *J. Chromatogr.* 347 (1985) 11.
- [28] L. Schweitz, P. Spegel, S. Nilsson, *Electrophoresis* 22 (2001) 4053.
- [29] Y.L. Xu, Z.S. Liu, H.F. Wang, C. Yan, R.Y. Gao, *Electrophoresis* 26 (2005) 804.
- [30] Q.L. Deng, Z.H. Lun, R.Y. Gao, L.H. Zhang, W.B. Zhang, Y.K. Zhang, *Electrophoresis* 27 (2006) 4351.
- [31] J. Matsui, T. Kato, T. Takeuchi, M. Suzuki, K. Yokoyama, E. Tamiya, I. Karube, *Anal. Chem.* 65 (1993) 2223.
- [32] E.C. Peters, M. Petro, F. Svec, J.M.J. Frechet, *Anal. Chem.* 70 (1998) 2296.
- [33] J.J. Ou, X. Li, S. Feng, J. Dong, X.L. Dong, L. Kong, M.L. Ye, H.F. Zou, *Anal. Chem.* 79 (2007) 639.
- [34] L. Rieux, H. Niederlander, E. Verpoorte, R. Bischoff, *J. Sep. Sci.* 28 (2005) 1628.
- [35] H.F. Wang, Y.Z. Zhu, X.P. Yan, R.Y. Gao, J.Y. Zheng, *Adv. Mater.* 18 (2006) 3266.
- [36] S. Laschober, M. Sulyok, E. Rosenberg, *J. Chromatogr. A* 1144 (2007) 55.
- [37] E. Dickinson, *Colloids Surf. B* 15 (1999) 161.
- [38] M. Glad, P. Reinholdsson, K. Mosbach, *React. Polym.* 25 (1995) 47.
- [39] M.Y. Wang, J. Xu, X. Zhou, T.W. Tan, *J. Chromatogr. A* 1147 (2007) 24.